

Polarforming for Wireless Communications: Modeling and Performance Analysis

Zijian Zhou, *Member, IEEE*, Jingze Ding, *Graduate Student Member, IEEE*, Chenbo Wang, *Member, IEEE*, Bingli Jiao, *Senior Member, IEEE*, and Rui Zhang, *Fellow, IEEE*

Abstract—This paper presents, for the first time, the concept of *polarforming* for wireless communications. Polarforming refers to a novel technique that enables dynamic adjustment of antenna polarization using reconfigurable polarized antennas (RPAs). It can fully leverage polarization diversity to improve the performance of wireless communication systems by aligning the effective polarization state of the incoming electromagnetic (EM) wave with the antenna polarization. To better demonstrate the benefits of polarforming, we propose a general RPA-aided system that allows for tunable antenna polarization. A wavefront-based channel model is developed to properly capture depolarization behaviors in both line-of-sight (LoS) and non-line-of-sight (NLoS) channels. Based on this model, we provide a detailed description of transmit and receive polarforming on planes of polarization (PoPs). We also evaluate the performance gains provided by polarforming under stochastic channel conditions. Specifically, we derive a closed-form expression for the relative signal-to-noise ratio (SNR) gain compared to conventional fixed-polarization antenna (FPA) systems and approximate the cumulative distribution function (CDF) for the RPA system. Our analysis reveals that polarforming offers a diversity gain of two, indicating full utilization of polarization diversity for dual-polarized antennas. Furthermore, extensive simulation results validate the effectiveness of polarforming and exhibit substantial improvements over conventional FPA systems. The results also indicate that polarforming not only can combat depolarization effects caused by wireless channels but also can overcome channel correlation when scattering is insufficient.

Index Terms—Polarforming, polarformer, reconfigurable polarized antenna (RPA), channel modeling, performance analysis.

I. INTRODUCTION

POLARIZATION describes the characteristics of an electromagnetic (EM) wave and theoretically, it holds the potential to triple channel capacity. The extra capacity arises from the existence of six distinct electric and magnetic polarization states at any given point [1]. Nonetheless, classical wireless systems place an overfull focus on optimizing time, frequency, and spatial resources, often neglecting polarization as another

dimension [2]–[4]. Although these systems have been successfully implemented, they are now reaching their theoretical and practical boundaries. To meet the unprecedented demands for higher data rates and more reliable connections, leveraging polarization diversity in wireless systems is becoming a promising and necessary evolution.

The polarization characteristics of wireless channels have been extensively investigated in the literature [5]–[9], which provide a solid foundation for understanding the impact of polarization on wireless communications. More specifically, the authors in [5] examined the mechanisms of depolarization for the non-line-of-sight (NLoS) channel from an electromagnetic perspective. They found that reflections, diffractions, and scattering of EM waves can cause significant changes in their polarization state and lead to depolarization. To quantify the degree of depolarization, cross-polarization discrimination (XPD) was introduced as the ratio of the average received power in the co-polar channel to that in the cross-polar channel [6]. The XPD provides a measurement of depolarization effects under different conditions. Further studies [7]–[9] measured the XPD in urban environments and showed that channel depolarization can result in a notable capacity degradation in practical wireless communication systems.

However, in the aforementioned studies, the antennas are deployed with a fixed polarization, called fixed-polarization antennas (FPAs). Since the events that cause depolarization, such as reflections, diffractions, and scattering, are random and highly dependent on the surrounding environment, conventional FPA systems cannot effectively adapt to channel variations or mitigate depolarization, particularly in complex scenarios like vehicular communications or unmanned aerial vehicle (UAV) networks [10], [11]. To overcome the inherent limitations of FPAs, reconfigurable polarized antennas (RPAs) are considered in this paper. RPAs allow for dynamic adjustment of antenna polarization in response to real-time channel conditions and depolarization effects. This capability provides better adaptability to a changing environment and enhances system performance in the presence of channel depolarization.

In the realm of antenna and propagation, the implementation of RPAs is well-established and beneficial for the advancement of antenna architecture. Various design approaches have been developed to enable reconfigurability of antenna polarization. For example, one widely used method involves electronic switches, such as positive intrinsic negative (PIN) diodes or microelectromechanical systems (MEMS), which can modify polarization angles and adjust radiation patterns [12]–[15]. Another method uses mechanical devices to achieve tunable

This work was jointly supported by the Science and Technology Project of Guangzhou under Grants 202206010118 and 2023B04J0011, and the National Natural Science Foundation of China under Grant 62171006. The calculations were supported by the High-Performance Computing Platform of Peking University. (*Corresponding authors: Zijian Zhou and Rui Zhang.*)

Z. Zhou, J. Ding, C. Wang, and B. Jiao are with the School of Electronics, Peking University, Beijing 100871, China (e-mail: zjzhou1008@pku.edu.cn; djz@stu.pku.edu.cn; {wcb15, jiaobl}@pku.edu.cn).

R. Zhang is with the School of Science and Engineering, Shenzhen Research Institute of Big Data, The Chinese University of Hong Kong, Shenzhen, Guangdong 518172, China (e-mail: rzhang@cuhk.edu.cn). He is also with the Department of Electrical and Computer Engineering, National University of Singapore, Singapore 117583 (e-mail: elezhang@nus.edu.sg).

control over an antenna's electrical properties by moving different components [16], [17]. Although these mechanically reconfigurable antennas offer more precise control and flexibility than electronic switches, they also introduce increased complexity and higher power consumption. In addition, novel materials like graphene metasurfaces and liquid metals have been investigated for creating more compact and flexible RPAs. Metasurfaces, in particular, have shown significant potential in applications involving single antennas [18], [19] and antenna arrays [20]–[22]. These materials allow antennas to achieve wideband operation and increased gain while maintaining a low profile. However, there is often a need to balance the cost of these materials with the precision of reconfiguration. To address such tradeoff, alternative designs, such as time-modulated patch antennas, utilize low-frequency signals to dynamically adjust surface currents, which facilitate controlled polarization changes and nonreciprocal responses [23]. These diverse solutions ensure the reconfigurability of antenna polarization through various antenna parameters across multiple frequency bands and are viable for integration into existing wireless communication systems. Besides reconfigurable antenna polarization, recent studies have also explored the antenna position/rotation adjustment for improving wireless communication system performances [24], [25].

There are several preliminary studies in the literature that explored the application of RPAs for wireless communications from various perspectives, including single-user multiple-input multiple-output (MIMO) [26], [27], multi-user MIMO [28], multi-hop communication [29], and wideband communication [30]. These studies demonstrated the advantages of RPAs in practical applications, but their focus is different from our work. Specifically, the fundamental aspects of channel modeling and a comprehensive analysis of the performance improvements provided by RPAs have not been thoroughly investigated in the aforementioned studies. In [26], for example, the authors explored the application of pattern-reconfigurable antennas in single-user MIMO systems by dynamically modifying radiation patterns. Meanwhile, an online learning-based approach for selecting antenna modes based on channel correlation was introduced in [27] to optimize communication links. For multi-user MIMO systems, the authors in [28] studied the effectiveness of radiation pattern reconfigurable antennas in mitigating interference and enhancing overall system robustness. In [29], the authors optimized the throughput of systems in multi-hop communication networks with the aid of pattern reconfigurable antennas, which can agilely switch among many different antenna radiation patterns. The use of linear polarization in wideband MIMO systems was proposed in [30], where the reconfigurable antennas act as an additional precoding step to optimize polarization states on unpolarized channels.

In light of the above, this paper aims to investigate the channel modeling and performance analysis of wireless communication systems enabled by RPAs. Unlike the aforementioned methods for implementing RPAs, we propose a simpler and more straightforward approach that employs phase shifters and attenuators, collectively called a *polarformer*. By adjusting the amplitude and phase of the signals, the antenna polarization can be changed accordingly. In conventional channel models,

little depolarization in the line-of-sight (LoS) channel is considered because the transmit and receive antennas are assumed to be perfectly aligned [31]. However, this assumption is not always practical in real-world applications, where antenna misalignment and environmental factors can lead to significant polarization mismatch. To address this limitation, we develop a wavefront-based channel model in this paper, which can capture the depolarization behaviors in both LoS and NLoS channels.

The main contributions of this paper are listed as follows.

- We present the concept of polarforming for wireless communications, a novel technique that uses RPAs to fully exploit polarization diversity. Transmit polarforming can modify the polarization state of EM waves by altering the transmit antenna polarization to match the receive antenna polarization. Conversely, receive polarforming enables dynamic adjustments of the receive antenna polarization to align with the effective polarization state of the incoming EM waves.
- We develop a wavefront-based channel model by leveraging the Euler angles and angle of arrival/angle of departure (AoA/AoD) information on each propagation path. Based on this model, we provide a detailed description of transmit and receive polarforming on planes of polarization (PoPs), and we analyze the degree of depolarization in both LoS and NLoS channels.
- We derive the relative signal-to-noise ratio (SNR) gain of the RPA system compared to the FPA systems under stochastic channel conditions. By using the Gauss-Chebyshev quadrature method, we further approximate the cumulative distribution function (CDF) of the maximum channel gain achievable by polarforming. In our analysis, polarforming can achieve a diversity gain of two and it indicates full utilization of polarization diversity for dual-polarized antennas. In addition, we discuss various considerations that may impact the effectiveness of polarforming in practical scenarios.
- We carry out extensive simulations to demonstrate the performance gains provided by polarforming in wireless communication systems under different channel conditions. The numerical results demonstrate that polarforming effectively mitigates channel depolarization and offers substantial improvements over the FPA systems.

The rest of this paper is organized as follows. Section II outlines the principles of EM wave propagation and introduces the wavefront-based channel model. In Section III, we focus on performance analysis of the RPA system, covering descriptions of polarforming, depolarization effects, and performance gains provided by polarforming. Section IV provides numerical results to verify the performance improvements of the RPA system over conventional FPA systems, and this paper is concluded in Section V.

Notation: a , \mathbf{a} , and \mathbf{A} denote a scalar, a vector, and a matrix, respectively. $(\cdot)^T$, $(\cdot)^*$, and $(\cdot)^H$ denote transpose, conjugate, and conjugate transpose, respectively. We use $\mathbb{E}\{\cdot\}$ for the mathematical expectation, $\tan^{-1}(\cdot)$ for an arctangent function, and $\text{mod}\{a, b\}$ for a modulo function that calculates

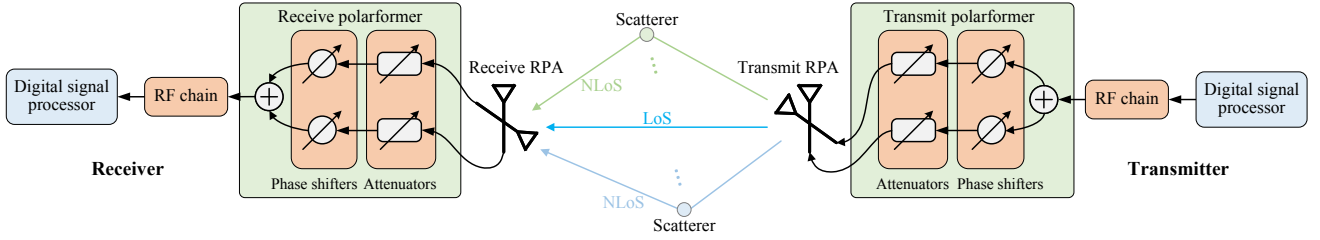


Fig. 1. A schematic for the wireless communication system with RPAs.

the remainder of the division a by b . $|\cdot|$ and $\angle(\cdot)$ denote the amplitude and phase of a complex number, respectively. $d(\cdot)$ denotes the differential of a function and $\|\cdot\|_F$ denotes the Frobenius norm. \mathbf{I}_L denotes an identical matrix of size $L \times L$, $\mathbf{A}^{1/2}$ denotes the square root of a matrix \mathbf{A} , and $\mathbf{a} \cdot \mathbf{b}$ denotes the dot product of vectors \mathbf{a} and \mathbf{b} . The symbol \triangleq defines a new variable. $\mathcal{CN}(0, \sigma^2)$ denotes the circularly symmetric complex Gaussian (CSCG) distribution with zero mean and variance of σ^2 , and $\mathcal{U}(a, b)$ denotes the uniform distribution over the interval $[a, b]$.

II. SYSTEM MODEL

As depicted in Fig. 1, we consider a general RPA-aided wireless communication system that can steer the antenna polarization through polarformers. The RPAs are assumed to be orthogonally dual-polarized and each consists of two linearly polarized elements oriented at right angles, i.e., \mathcal{V} -element for vertical polarization and \mathcal{H} -element for horizontal polarization.

A. Preliminaries

From the perspective of electromagnetism, an EM wave propagating in free space is described as a transverse wave. This means that the radiated electric and magnetic fields have no component along the direction of propagation. Instead, they are perpendicular to one another on a transverse wavefront as well as to the direction of propagation. The magnetic field is associated with the electric field through a ninety-degree phase shift and its strength depends on the wave impedance of the medium. Once the propagation direction is fixed, only two degrees of freedom (DoFs) remain. Consequently, a two-dimensional complex vector, called the Jones vector, is used to characterize the polarization nature of the electric fields. It is a function of time t and spatial position z , given by

$$\vec{E}(z, t) = [E_x, E_y]^T e^{j(kz - \omega t)}, \quad (1)$$

where k is the wavenumber and ω is the angular frequency of the EM wave. The complex values E_x and E_y represent electric field components along the orthogonal x and y directions on the wavefront, respectively. The polarization state of an EM wave is determined by the amplitudes and the phase difference of its electric field components. To account for the polarization state using the Jones vector, an example including different types of polarization is provided in Fig. 2, where $\zeta = \angle E_x - \angle E_y$ denotes the phase difference of the components.

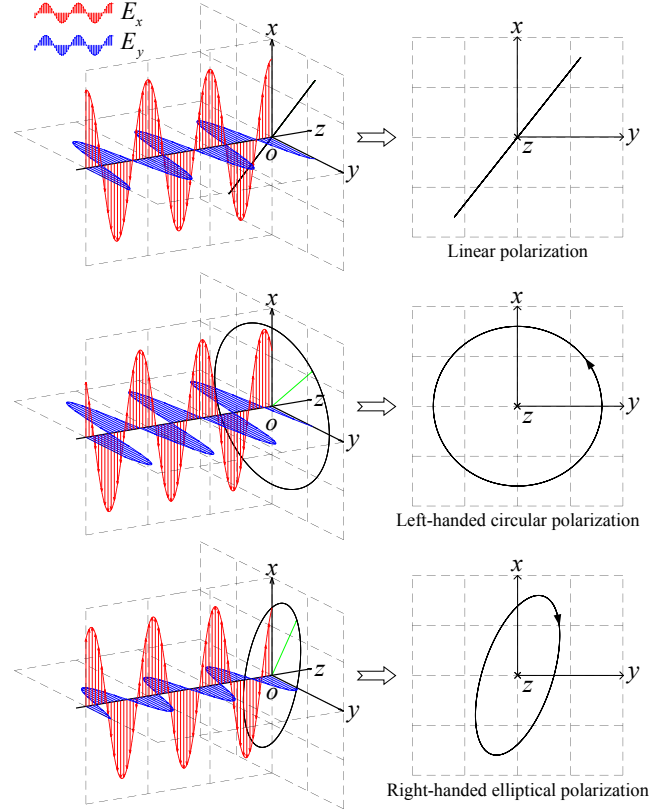


Fig. 2. An example for the polarization state of three given types, i.e., linear polarization ($|E_x| = 0.8$, $|E_y| = 0.6$, and $\zeta = 0$), left-handed circular polarization ($|E_x| = 0.8$, $|E_y| = 0.8$, and $\zeta = -\pi/2$), and right-handed elliptical polarization ($|E_x| = 0.8$, $|E_y| = 0.4$, and $\zeta = \pi/3$). The left side shows a diagram of EM waves propagating over time and the right side depicts the PoPs on the wavefront.

B. Achieving Tunability

According to Maxwell's equations, EM waves arise from oscillating charges, which result in time-varying currents. In electrostatics, the electric field is proportional to the static charge density, as described by Gauss's law, while in magnetostatics, the magnetic field is proportional to the steady current density, as described by Ampère's law. For simplicity, we omit the proportionality constants. Thus, the orthogonal electric field components generated on the transmit RPA are denoted in the form of the Jones vector, i.e., $\mathbf{f}(\mathbf{t})\sqrt{P_t}s$, where P_t is the transmit power and s is the transmitted signal with zero mean and normalized power of one. The vector $\mathbf{f}(\mathbf{t})$, referred to as the transmit polarforming vector (PFV), is given

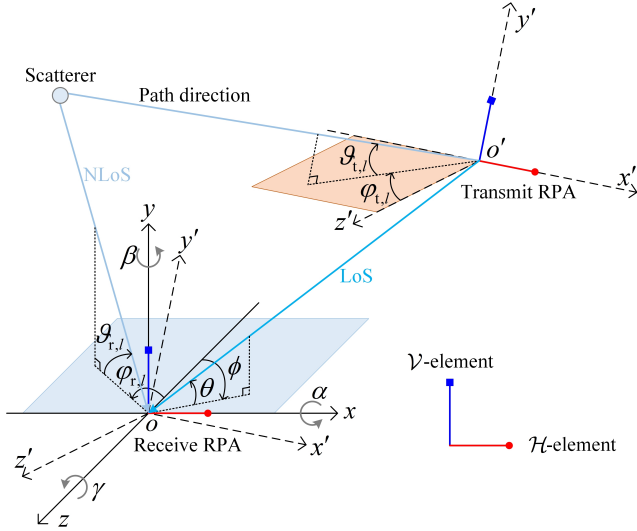


Fig. 3. Illustration of the right-handed Cartesian coordinate systems and spatial angles for the RPA system.

by

$$\mathbf{f}(\mathbf{t}) = [\cos \rho_t, \sin \rho_t e^{-j\psi_t}]^T, \quad (2)$$

in terms of its amplitude-phase vector (APV), defined as $\mathbf{t} = [\rho_t, \psi_t]^T$. Similarly, the receive PFV in terms of its APV, $\mathbf{r} = [\rho_r, \psi_r]^T$, is denoted as

$$\mathbf{g}(\mathbf{r}) = [\cos \rho_r, \sin \rho_r e^{-j\psi_r}]^T. \quad (3)$$

In (2) and (3), ρ_t and ρ_r represent the amplitude coefficients for the \mathcal{V} - and \mathcal{H} -elements of the corresponding RPA (in the form of phase angles), respectively. Also, ψ_t and ψ_r represent the phase differences between the elements. Note that the vectors, $\mathbf{f}(\mathbf{t})$ and $\mathbf{g}(\mathbf{r})$, indicate the polarization of transmit and receive RPAs, respectively. As shown in Fig. 1, the tunability of antenna polarization is enabled by phase shifters and attenuators in the transmit and receive polarformers. Without loss of generality, the tunable ranges of these parameters are assumed to be $\rho_t, \rho_r \in [0, \pi/2]$ and $\psi_t, \psi_r \in [0, 2\pi)$, which correspond to the tunable region \mathcal{C}_p for the transmit and receive APVs with $\mathbf{t}, \mathbf{r} \in \mathcal{C}_p$.

For the considered RPA system, the channel response is a function of the transmit and receive APVs, i.e., $h(\mathbf{t}, \mathbf{r})$. Therefore, the received signal at the receiver is expressed as

$$\mathbf{r}(\mathbf{t}, \mathbf{r}) = h(\mathbf{t}, \mathbf{r}) \sqrt{P_t} \mathbf{s} + n \triangleq \mathbf{g}(\mathbf{r})^H \mathbf{H} \mathbf{f}(\mathbf{t}) \sqrt{P_t} \mathbf{s} + n, \quad \mathbf{t}, \mathbf{r} \in \mathcal{C}_p, \quad (4)$$

where n is the additive white Gaussian noise with zero mean and power of δ^2 . The channel matrix \mathbf{H} of two-by-two dimensions, is composed of an LoS component and an NLoS component, i.e., $\mathbf{H} = \bar{\mathbf{H}} + \tilde{\mathbf{H}}$, which are subsequently derived in Section II-C.

As a result, the SNR of the received signal is given by

$$\gamma(\mathbf{t}, \mathbf{r}) = \frac{|h(\mathbf{t}, \mathbf{r})|^2 P_t}{\delta^2}, \quad \mathbf{t}, \mathbf{r} \in \mathcal{C}_p. \quad (5)$$

C. Wavefront-based Channel Model

To illustrate the spatial relationships between the transmit and receive RPAs, a global coordinate system (GCS), x - y - z , and a local coordinate system (LCS), x' - y' - z' , are established as shown in Fig. 3, where the fixed LoS and scattering NLoS paths combine to form the incoming EM waves. In these coordinate systems, the \mathcal{V} -element is oriented in the positive y - or y' -direction with unit vector $\mathbf{y} = [0, 1, 0]^T$ and the \mathcal{H} -element in the positive x - or x' -direction with unit vector $\mathbf{x} = [1, 0, 0]^T$. Generally, the polarization of the elements corresponds to the orientation of the electric field oscillations. For convenience, the notations s_x and c_x in this subsection denote trigonometric functions $\sin(x)$ and $\cos(x)$, respectively. Under these setups, the channel modeling of the LoS and NLoS components is developed based on the wavefront of EM waves in the following derivations.

First, we denote the elevation and azimuth AoAs for the LoS path as $\theta \in [-\Theta/2, \Theta/2]$ and $\phi \in [-\Phi/2, \Phi/2]$, respectively, where Θ and Φ are fixed coverage angles that, in principle, do not exceed π . The physical AoAs of the LoS path also indicate the direction of the transmit RPA. As we have discussed in Section II-A, the polarization state of an EM wave can be described by any two orthogonal electric field components on the wavefront with no component along the LoS path. The orthogonal unit vectors in the GCS, $\mathbf{u} = [s_\theta s_\phi, -c_\theta, s_\theta c_\phi]^T$ and $\mathbf{v} = [c_\phi, 0, -s_\phi]^T$, are chosen to identify the polarization state of the EM wave traveling along the LoS path. Viewed from the LCS, the vectors \mathbf{u}' and \mathbf{v}' results from the coordinate rotation of \mathbf{u} and \mathbf{v} through a coordinate rotation matrix \mathbf{R} , such that $\mathbf{u}' = \mathbf{R}\mathbf{u}$ and $\mathbf{v}' = \mathbf{R}\mathbf{v}$. Both \mathbf{u}' and \mathbf{v}' are respectively parallel to \mathbf{u} and \mathbf{v} , and remain perpendicular to each other as well as to the LoS path. The coordinate rotation matrix is given by [32]

$$\mathbf{R} = \begin{bmatrix} c_\beta c_\gamma & c_\beta s_\gamma & -s_\beta \\ s_\alpha s_\beta c_\gamma - c_\alpha s_\gamma & s_\alpha s_\beta s_\gamma + c_\alpha c_\gamma & s_\alpha c_\beta \\ c_\alpha s_\beta c_\gamma + s_\alpha s_\gamma & c_\alpha s_\beta s_\gamma - s_\alpha c_\gamma & c_\alpha c_\beta \end{bmatrix}, \quad (6)$$

where α, β, γ are Euler angles with respect to axes x, y, z , respectively.

The electric field components of the LoS path are achieved by projecting the time-varying electric fields of the transmit RPA onto the wavefront of the LoS path [33]. The projection matrix that captures this transformation can be obtained using the vectors \mathbf{u}' and \mathbf{v}' , as shown in (7) at the top of the next page. The received fields are similarly obtained by projecting the components of the wavefront onto the receive RPA through the projection matrix given by

$$\mathbf{Q} = \begin{bmatrix} \mathbf{u} \cdot \mathbf{y} & \mathbf{v} \cdot \mathbf{y} \\ \mathbf{u} \cdot \mathbf{x} & \mathbf{v} \cdot \mathbf{x} \end{bmatrix} = \begin{bmatrix} -c_\theta & 0 \\ s_\theta s_\phi & c_\phi \end{bmatrix}. \quad (8)$$

The polarization state of an EM wave is assumed to be consistent as it travels through the LoS path¹. Thus, the

¹For the LoS channel, propagation in the presence of rain, snow, or hail can create depolarization. In such cases, the polarization state of an EM wave traveling along the LoS path may change, which necessitates the consideration of a depolarization matrix in the channel matrix (9).

$$\mathbf{P} = \begin{bmatrix} \mathbf{y} \cdot \mathbf{u}' & \mathbf{x} \cdot \mathbf{u}' \\ \mathbf{y} \cdot \mathbf{v}' & \mathbf{x} \cdot \mathbf{v}' \end{bmatrix} = \begin{bmatrix} s_\alpha s_\beta c_\gamma s_\theta s_\phi - c_\alpha s_\gamma s_\theta s_\phi - s_\alpha s_\beta s_\gamma c_\theta - c_\alpha c_\gamma c_\theta + s_\alpha c_\beta s_\theta c_\phi & c_\beta c_\gamma s_\theta s_\phi - c_\beta s_\gamma c_\theta - s_\beta s_\theta c_\phi \\ s_\alpha s_\beta c_\gamma c_\phi - c_\alpha s_\gamma c_\phi - s_\alpha c_\beta s_\phi & c_\beta c_\gamma c_\phi + s_\beta s_\phi \end{bmatrix}. \quad (7)$$

channel matrix of the LoS component is given by

$$\tilde{\mathbf{H}} = \mathbf{Q}\mathbf{P}\boldsymbol{\nu} \triangleq \begin{bmatrix} a_{\mathcal{V}\mathcal{V}} & a_{\mathcal{H}\mathcal{V}} \\ a_{\mathcal{V}\mathcal{H}} & a_{\mathcal{H}\mathcal{H}} \end{bmatrix} \boldsymbol{\nu}, \quad (9)$$

where $\boldsymbol{\nu}$ is a complex scale factor for free-space path loss, and $a_{ij\nu}$ represents the channel coefficient from the i -element of the transmit RPA to the j -element of the receive RPA for $i, j \in \{\mathcal{V}, \mathcal{H}\}$.

Next, let us move to the NLoS channel. We consider a general geometric channel model, in which the transmit and receive paths have one-to-one correspondence. For the l -th path, the elevation and azimuth AoDs and AoAs are denoted as $\vartheta_{t,l}$, $\varphi_{t,l}$, $\vartheta_{r,l}$, and $\varphi_{r,l}$, respectively, where $\vartheta_{t,l}, \varphi_{t,l}, \vartheta_{r,l}, \varphi_{r,l} \in [-\pi/2, \pi/2]$. Here, $l = 1, 2, \dots, L$, where L is the number of scattering paths. The orthogonal vectors perpendicular to the l -th path at the transmitter and receiver are given by $\mathbf{u}_{t,l} = [s_{\vartheta_{t,l}} s_{\varphi_{t,l}}, -c_{\vartheta_{t,l}}, s_{\vartheta_{t,l}} c_{\varphi_{t,l}}]^T$, $\mathbf{v}_{t,l} = [c_{\varphi_{t,l}}, 0, -s_{\varphi_{t,l}}]^T$, $\mathbf{u}_{r,l} = [s_{\vartheta_{r,l}} s_{\varphi_{r,l}}, -c_{\vartheta_{r,l}}, s_{\vartheta_{r,l}} c_{\varphi_{r,l}}]^T$, and $\mathbf{v}_{r,l} = [c_{\varphi_{r,l}}, 0, -s_{\varphi_{r,l}}]^T$, respectively. Similar to the derivations for the LoS channel, the projection matrices for transmission and reception along the l -th NLoS path are respectively given by

$$\mathbf{T}_{t,l} = \begin{bmatrix} \mathbf{y} \cdot \mathbf{u}_{t,l} & \mathbf{x} \cdot \mathbf{u}_{t,l} \\ \mathbf{y} \cdot \mathbf{v}_{t,l} & \mathbf{x} \cdot \mathbf{v}_{t,l} \end{bmatrix} = \begin{bmatrix} -c_{\vartheta_{t,l}} & s_{\vartheta_{t,l}} s_{\varphi_{t,l}} \\ 0 & c_{\varphi_{t,l}} \end{bmatrix}, \quad (10)$$

$$\mathbf{T}_{r,l} = \begin{bmatrix} \mathbf{u}_{r,l} \cdot \mathbf{y} & \mathbf{v}_{r,l} \cdot \mathbf{y} \\ \mathbf{u}_{r,l} \cdot \mathbf{x} & \mathbf{v}_{r,l} \cdot \mathbf{x} \end{bmatrix} = \begin{bmatrix} -c_{\vartheta_{r,l}} & 0 \\ s_{\vartheta_{r,l}} s_{\varphi_{r,l}} & c_{\varphi_{r,l}} \end{bmatrix}. \quad (11)$$

For the NLoS channel, EM waves encounter obstacles or scatterers that can cause reflection, diffraction, or scattering. These interactions can deflect the electric field into different polarization states, thereby leading to depolarization [6]. Therefore, a depolarization matrix, defined as $\boldsymbol{\Sigma}_l$ of two-by-two dimensions for $l = 1, 2, \dots, L$, is essential to account for depolarization effects. With this, the channel matrix of the NLoS component is given by

$$\tilde{\mathbf{H}} = \sum_{l=1}^L \mathbf{T}_{r,l} \boldsymbol{\Sigma}_l \mathbf{T}_{t,l} \triangleq \begin{bmatrix} d_{\mathcal{V}\mathcal{V}} & d_{\mathcal{H}\mathcal{V}} \\ d_{\mathcal{V}\mathcal{H}} & d_{\mathcal{H}\mathcal{H}} \end{bmatrix}, \quad (12)$$

where d_{ij} represents the channel coefficient from the i -element of the transmit RPA to the j -element of the receive RPA for $i, j \in \{\mathcal{V}, \mathcal{H}\}$.

Note that the mechanism of depolarization in the NLoS channel is extremely complicated because the events causing depolarization are random and dependent on the surrounding environment. This complexity makes it difficult for the elements of the depolarization matrix, $\boldsymbol{\Sigma}_l$ for $l = 1, 2, \dots, L$, to conform to a typical distribution. Nevertheless, if the number of scattering paths approaches infinity and the elements of $\tilde{\mathbf{H}}$ are independent and identically distributed (i.i.d.) random variables, the central limit theory suggests these elements are i.i.d. CSCG-distributed random variables, regardless of the original distribution of the variables.

III. PERFORMANCE ANALYSIS

To better evaluate the performance gain of the considered RPA system compared to the conventional FPA system, we consider a simplified scenario where the transmit APV is fixed at $\mathbf{t}_0 = [\rho_{t_0}, \psi_{t_0}]^T$ while the receive APV remains flexible. In this setup, the channel response is simplified to

$$h(\mathbf{r}) = \mathbf{g}(\mathbf{r})^H \mathbf{b} = b_1 \cos \rho_r + b_2 \sin \rho_r e^{j\psi_{\rho_r}}, \quad \mathbf{r} \in \mathcal{C}_p, \quad (13)$$

where $\mathbf{b} = \mathbf{H}\mathbf{f}(\mathbf{t}_0) \triangleq [b_1, b_2]^T$, referred to as the effective polarization state vector (EPSV), represents the effective polarization state of the incoming EM wave. As the channel response depends on the configuration of the receive PFV, the received SNR in (5) varies accordingly. In this section, we provide a detailed illustration for transmit and receive polarforming and a comprehensive description of the depolarization effects in both LoS and NLoS channels. Furthermore, we analyze the performance improvements offered by a single receive polarformer under stochastic channel conditions, followed by a discussion of practical considerations.

A. Transmit and Receive Polarforming

In this subsection, we explore the properties of transmit and receive polarforming for the deterministic channel with a given EPSV. We start by considering a fixed transmit APV and then perform receive polarforming. Therefore, for a given EPSV, the channel (power) gain can be expressed as

$$|h(\mathbf{r})|^2 = |b_1|^2 \cos^2 \rho_r + |b_2|^2 \sin^2 \rho_r + |b_1| |b_2| \sin 2\rho_r \cos(\psi_r + \omega_2 - \omega_1), \quad \mathbf{r} \in \mathcal{C}_p, \quad (14)$$

where $\omega_\ell = \angle b_\ell$, $\ell = 1, 2$. The range of $\psi_r + \omega_2 - \omega_1$ varies from $\omega_1 - \omega_2$ to $2\pi + \omega_1 - \omega_2$. Due to $|b_1| |b_2| \sin 2\rho_r \geq 0$ for $\rho_r \in [0, \pi/2]$, the maximum value for the third term in (14) can be found by setting $\psi_r = \text{mod}\{\omega_1 - \omega_2, 2\pi\}$, which yields

$$\begin{aligned} |h(\mathbf{r})|^2 &\leq |b_1|^2 \cos^2 \rho_r + |b_2|^2 \sin^2 \rho_r + |b_1| |b_2| \sin 2\rho_r \\ &= (|b_1| \cos \rho_r + |b_2| \sin \rho_r)^2 \\ &\leq |b_1|^2 + |b_2|^2. \end{aligned} \quad (15)$$

The last inequality is satisfied by using the Cauchy-Schwarz inequality. Thus, the maximum channel gain achieved by receive polarforming is given by

$$\max_{\mathbf{r} \in \mathcal{C}_r} |h(\mathbf{r})|^2 = |b_1|^2 + |b_2|^2, \quad (16)$$

with the optimal configuration of the receive APV given by

$$\begin{cases} \rho_r^{\max} = \tan^{-1}(|b_2|/|b_1|), \\ \psi_r^{\max} = \text{mod}\{\omega_1 - \omega_2, 2\pi\}. \end{cases} \quad (17)$$

Similarly, the minimum channel gain can be obtained by receive polarforming as

$$\min_{\mathbf{r} \in \mathcal{C}_r} |h(\mathbf{r})|^2 = \min_{0 \leq \rho_r \leq \frac{\pi}{2}} (|b_1| \cos \rho_r - |b_2| \sin \rho_r)^2 = 0. \quad (18)$$

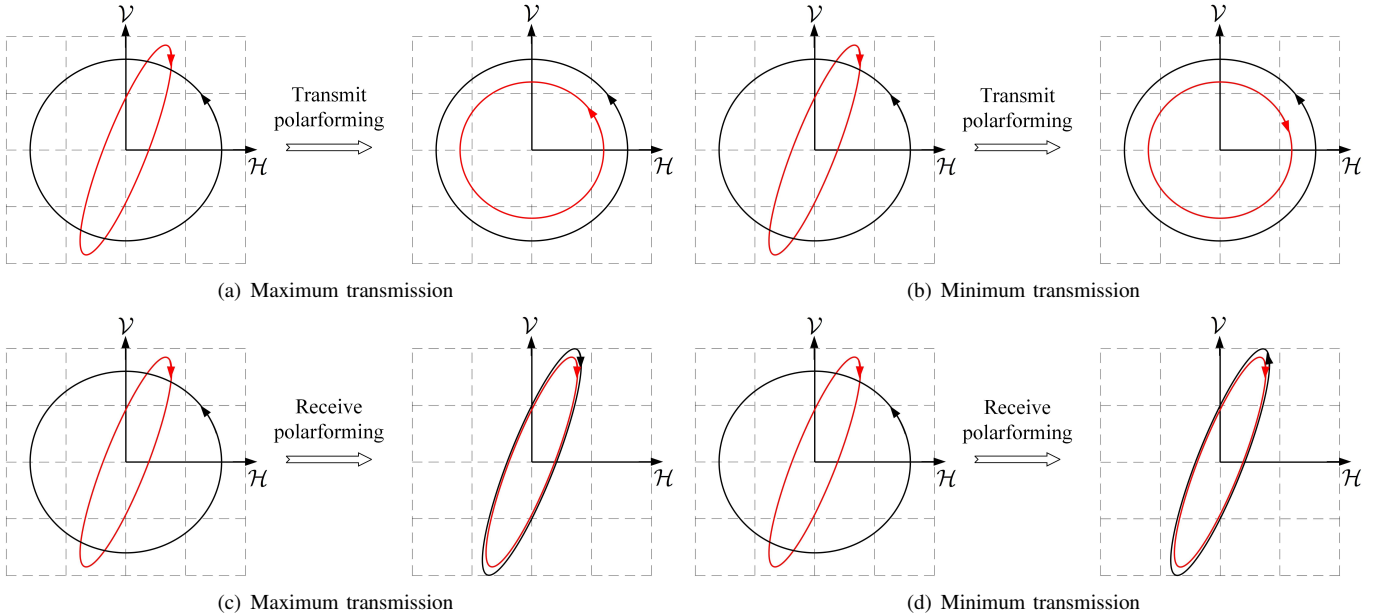


Fig. 4. Illustration of transmit and receive polarforming via PoPs with the original EPSV given by $|b_1| = \sin(3\pi/8)$, $|b_2| = \cos(3\pi/8)$, and $\omega_1 - \omega_2 = \pi/6$. The black line shows the receive antenna polarization (determined by the receive APV) and the effective polarization state of the incoming EM wave is highlighted in red.

The corresponding receive APV for (18) is configured as

$$\begin{cases} \rho_r^{\min} = \tan^{-1}(|b_1|/|b_2|), \\ \psi_r^{\min} = \text{mod}\{\pi + \omega_1 - \omega_2, 2\pi\}. \end{cases} \quad (19)$$

While the above configurations are based on receive polarforming, transmit polarforming can be operated in a similar manner. As can be seen from (18), a zero channel gain can be achieved through polarforming. In other words, the transmit and receive RPAs can always be configured to be orthogonal to each other, regardless of the channel conditions. This property may have potential benefits for wireless systems and applications where minimizing interference is crucial, such as secure communication systems and interference-nulling techniques.

An illustrative example for transmit and receive polarforming is provided in Fig. 4, where the original EPSV (without polarforming) is fixed with parameters $|b_1| = \sin(3\pi/8)$, $|b_2| = \cos(3\pi/8)$, and $\omega_1 - \omega_2 = \pi/6$. The left side of each figure shows the effective polarization state of the incoming EM wave and the fixed antenna polarization (e.g., left-handed circular polarization), and in contrast, the right side displays these states achieved through polarforming. In these figures, transmit polarforming achieves polarization matching by modifying the polarization state of the EM wave to align with the receive antenna polarization. Conversely, receive polarforming alters the antenna polarization to match the effective polarization state of the incoming EM wave. This polarization matching ensures the maximum or minimum channel gain for the RPA-aided wireless communication systems. It can also be seen that the distinction between maximum and minimum transmissions is only due to the opposite rotation direction of the polarized ellipse or circle.

B. Channel Depolarization

We analyze the depolarization effects of the LoS and NLoS channels in this subsection based on the proposed wavefront-based channel model.

1) *Depolarization of the LoS channel:* Conventional channel models assume no or negligible depolarization for the LoS channel by considering a simplified scenario where the transmit and receive polarized antennas are perfectly aligned. In other words, the Euler angles and physical AoAs of the LoS path are equal to zero, i.e., $\alpha, \beta, \gamma, \theta, \phi = 0$. Under this setup, the entries of the channel matrix \mathbf{H} have fixed phase shifts only [31]. However, in practical systems, the transmit and receive polarized antennas are often not perfectly aligned because of random deployment and there exists additional depolarization due to their spatial relationships.

The proposed wavefront-based channel model in (9) is well-suited to accurately capture the depolarization caused by the misalignment of antenna orientations. As defined in Section II-C, the Euler angles α, β, γ represent the relative orientations between the transmit and receive antennas, while the physical AoAs of the LoS path indicate the direction of the transmit antenna. Without loss of generality, we assume that the Euler angles are i.i.d. and uniformly distributed over the intervals $[0, 2\pi)$, and the AoAs of the LoS path are i.i.d. and uniformly distributed with $\theta \sim \mathcal{U}(-\Theta/2, \Theta/2)$ and $\phi \sim \mathcal{U}(-\Phi/2, \Phi/2)$. Recalling that Θ and Φ are the coverage angles in elevation and azimuth directions, respectively, we assume $\Theta, \Phi \in [0, \pi]$, which defines the range of possible incoming wave directions of the LoS path. Under these assumptions, we evaluate the average degree of depolarization for the LoS channel in the following.

For simplicity, we assume that $\nu = 1$ and the entry of \mathbf{P} in its i -th row and j -th column is denoted as p_{ij} , $i, j = 1, 2$.

To obtain the average degree of depolarization for the LoS channel, we calculate the expected values of the channel gains for the co-polar and cross-polar channels as follows.

$$\begin{aligned}\mathbb{E}\{a_{\mathcal{V}\mathcal{V}}^2\} &= \mathbb{E}\{c_\theta^2 p_{11}^2\} \\ &= \frac{1}{4}\dot{s}_\alpha\dot{s}_\beta\dot{c}_\gamma\dot{s}_{2\theta}\dot{s}_\phi + \frac{1}{4}\dot{c}_\alpha\dot{s}_\gamma\dot{s}_{2\theta}\dot{s}_\phi \\ &\quad + \dot{s}_\alpha\dot{s}_\beta\dot{s}_\gamma\dot{c}_\theta + \dot{c}_\alpha\dot{c}_\gamma\dot{c}_\theta + \frac{1}{4}\dot{s}_\alpha\dot{c}_\beta\dot{s}_{2\theta}\dot{c}_\phi \\ &= \frac{3}{32}\dot{S}_{2\Theta}\dot{S}_\Phi + \frac{3}{8}\dot{C}_\Theta + \frac{1}{16}\dot{S}_{2\Theta}\dot{C}_\Phi \triangleq \lambda_{11}^2, \quad (20)\end{aligned}$$

$$\begin{aligned}\mathbb{E}\{a_{\mathcal{H}\mathcal{V}}^2\} &= \mathbb{E}\{c_\theta^2 p_{12}^2\} \\ &= \frac{1}{4}\dot{c}_\beta\dot{c}_\gamma\dot{s}_{2\theta}\dot{s}_\phi + \dot{c}_\beta\dot{s}_\gamma\dot{c}_\theta + \frac{1}{4}\dot{s}_\beta\dot{s}_{2\theta}\dot{c}_\phi \\ &= \frac{1}{16}\dot{S}_{2\Theta}\dot{S}_\Phi + \frac{1}{4}\dot{C}_\Theta + \frac{1}{8}\dot{S}_{2\Theta}\dot{C}_\Phi \triangleq \lambda_{12}^2, \quad (21)\end{aligned}$$

$$\begin{aligned}\mathbb{E}\{a_{\mathcal{V}\mathcal{H}}^2\} &= \mathbb{E}\{s_\theta^2 s_\phi^2 p_{11}^2 + c_\phi^2 p_{21}^2 + 2s_\theta s_\phi c_\phi p_{11} p_{21}\} \\ &= \dot{s}_\alpha\dot{s}_\beta\dot{c}_\gamma\dot{s}_\theta\dot{s}_\phi + \dot{c}_\alpha\dot{c}_\gamma\dot{s}_\theta\dot{s}_\phi + \frac{1}{4}\dot{s}_\alpha\dot{s}_\beta\dot{s}_\gamma\dot{s}_{2\theta}\dot{s}_\phi \\ &\quad + \frac{1}{4}\dot{c}_\alpha\dot{c}_\gamma\dot{s}_{2\theta}\dot{s}_\phi + \frac{1}{4}\dot{s}_\alpha\dot{c}_\beta\dot{s}_\theta\dot{s}_{2\phi} + \dot{s}_\alpha\dot{s}_\beta\dot{c}_\gamma\dot{c}_\phi \\ &\quad + \dot{c}_\alpha\dot{s}_\gamma\dot{c}_\phi + \frac{1}{4}\dot{s}_\alpha\dot{c}_\beta\dot{s}_{2\phi} + \frac{1}{2}\dot{s}_\alpha\dot{s}_\beta\dot{c}_\gamma\dot{s}_\theta\dot{s}_{2\phi} \\ &= \frac{3}{8}\dot{S}_\Theta\dot{S}_\Phi + \frac{3}{32}\dot{S}_{2\Theta}\dot{S}_\Phi + \frac{1}{16}\dot{S}_\Theta\dot{S}_{2\Phi} \\ &\quad + \frac{3}{8}\dot{C}_\Phi + \frac{1}{16}\dot{S}_{2\Phi} + \frac{1}{16}\dot{S}_\Theta\dot{S}_{2\Phi} \triangleq \lambda_{21}^2, \quad (22)\end{aligned}$$

$$\begin{aligned}\mathbb{E}\{a_{\mathcal{H}\mathcal{H}}^2\} &= \mathbb{E}\{s_\theta^2 s_\phi^2 p_{12}^2 + c_\phi^2 p_{22}^2 + 2s_\theta s_\phi c_\phi p_{12} p_{22}\} \\ &= \dot{c}_\beta\dot{c}_\gamma\dot{s}_\theta\dot{s}_\phi + \frac{1}{4}\dot{c}_\beta\dot{s}_\gamma\dot{s}_{2\theta}\dot{s}_\phi + \frac{1}{4}\dot{s}_\beta\dot{s}_\theta\dot{s}_{2\phi} + \dot{c}_\beta\dot{c}_\gamma\dot{c}_\phi \\ &\quad + \frac{1}{4}\dot{s}_\beta\dot{s}_{2\phi} + \frac{1}{2}\dot{c}_\beta\dot{c}_\gamma\dot{s}_\theta\dot{s}_{2\phi} - \frac{1}{2}\dot{s}_\beta\dot{s}_\theta\dot{s}_{2\phi} \\ &= \frac{1}{4}\dot{S}_\Theta\dot{S}_\Phi + \frac{1}{16}\dot{S}_{2\Theta}\dot{S}_\Phi + \frac{1}{8}\dot{S}_\Theta\dot{S}_{2\Phi} \\ &\quad + \frac{1}{4}\dot{C}_\Phi + \frac{1}{8}\dot{S}_{2\Phi} - \frac{1}{8}\dot{S}_\Theta\dot{S}_{2\Phi} \triangleq \lambda_{22}^2. \quad (23)\end{aligned}$$

The defined λ_{ij} is the entry of the average polarization matrix $\mathbf{\Lambda}$ in the i -th row and j -th column. The notations \dot{c}_x , \dot{s}_x , \ddot{c}_x , and \ddot{s}_x are respectively defined as $\dot{c}_x \triangleq \frac{1}{b-a} \int_a^b \cos^2(x) dx$, $\dot{s}_x \triangleq \frac{1}{b-a} \int_a^b \sin^2(x) dx$, $\ddot{c}_x \triangleq \frac{1}{b-a} \int_a^b \cos^4(x) dx$, and $\ddot{s}_x \triangleq \frac{1}{b-a} \int_a^b \sin^4(x) dx$, where x ranges from a to b . Leveraging trigonometric identities, we can easily find $\dot{c}_x = \dot{s}_x = \frac{1}{2}$ for all $x \in \{\alpha, \beta, \gamma\}$. Besides, $\dot{c}_x = \dot{C}_y$, $\dot{s}_x = \dot{S}_y$, $\ddot{c}_x = \ddot{C}_y$, and $\ddot{s}_x = \ddot{S}_y$ for $x \in \{\theta, \phi, 2\theta, 2\phi\}$ corresponding to $y \in \{\Theta, \Phi, 2\Theta, 2\Phi\}$. The notations \dot{C}_y , \dot{S}_y , \ddot{C}_y , and \ddot{S}_y are defined as $\dot{C}_y = \frac{1}{2} + \frac{1}{y} \sin \frac{y}{2} \cos \frac{y}{2}$, $\dot{S}_y = \frac{1}{2} - \frac{1}{y} \sin \frac{y}{2} \cos \frac{y}{2}$, $\ddot{C}_y = \frac{3}{8} + \frac{1}{2y} \sin \frac{y}{2} \cos^3 \frac{y}{2} + \frac{3}{4y} \sin \frac{y}{2} \cos \frac{y}{2}$, and $\ddot{S}_y = \frac{3}{8} - \frac{1}{2y} \sin^3 \frac{y}{2} \cos \frac{y}{2} - \frac{3}{4y} \sin \frac{y}{2} \cos \frac{y}{2}$. Additionally, we can find the cross-term is zero, i.e., $\mathbb{E}\{a_{ij} a_{mn}\} = 0$, $i, j, m, n \in \{\mathcal{V}, \mathcal{H}\}$ for $ij \neq mn$. It indicates that the elements in the matrix \mathbf{H} are i.i.d. random variables.

Furthermore, the XPD and co-polar ratio (CPR) are important metrics that provide valuable insights into the depolarization behavior of wireless channels. Specifically, the XPD measures the ratio of the expected channel gain in a co-polar

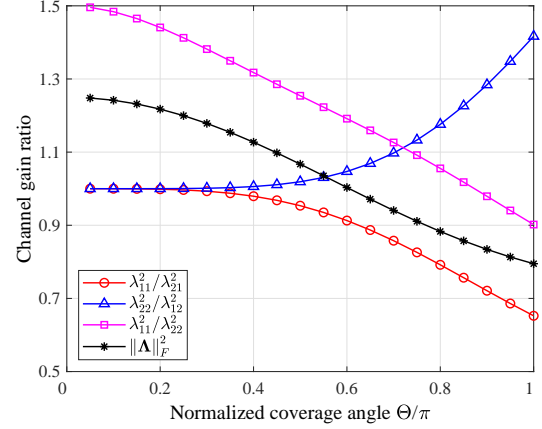


Fig. 5. Average degree of depolarization for the LoS channel versus the normalized coverage angle under the assumption of $\Theta = \Phi$.

channel to that in a cross-polar channel, while CPR measures the ratio of expected channel gain between the two co-polar channels. For random Euler angles and AoAs, the average \mathcal{V} -to- \mathcal{H} and \mathcal{H} -to- \mathcal{V} XPD are given by $\mathbb{E}\{a_{\mathcal{V}\mathcal{V}}^2\}/\mathbb{E}\{a_{\mathcal{V}\mathcal{H}}^2\} = \lambda_{11}^2/\lambda_{21}^2$ and $\mathbb{E}\{a_{\mathcal{H}\mathcal{H}}^2\}/\mathbb{E}\{a_{\mathcal{H}\mathcal{V}}^2\} = \lambda_{22}^2/\lambda_{12}^2$, respectively. The CPR is calculated by $\mathbb{E}\{a_{\mathcal{V}\mathcal{V}}^2\}/\mathbb{E}\{a_{\mathcal{H}\mathcal{H}}^2\} = \lambda_{11}^2/\lambda_{22}^2$. An illustrative example of the average degree of depolarization for the LoS channel is provided in Fig. 5, where the coverage angles are assumed to be $\Theta = \Phi$. In the figure, compared to the scenario with perfectly aligned antennas, i.e., $\mathbf{\Lambda} = \mathbf{I}_2$, the imbalances in XPD and CPR can be observed, which highlight the impact of polarization mismatch on the LoS channel. As the coverage angle increases, the \mathcal{V} -to- \mathcal{H} XPD decreases, while the \mathcal{H} -to- \mathcal{V} XPD exhibits an opposite trend and increases. Similarly, the CPR decreases with an increasing coverage angle, which indicates that the relative channel power in the \mathcal{V} -polar channel compared to the \mathcal{H} -polar channel diminishes. In addition, it can be seen that the square of the Frobenius norm, $\|\mathbf{\Lambda}\|_F^2$, is less than that of an identity matrix, i.e., $\|\mathbf{\Lambda}\|_F^2 < \|\mathbf{I}_2\|_F^2 = 2$. This result implies an overall loss in channel power, which further indicates that the LoS channel may experience performance degradation due to polarization mismatch.

We summarize the results in the following theorem to facilitate the analysis of the average system performance for the LoS channel.

Theorem 1: If the Euler angles and the AoAs are i.i.d. random variables and uniformly distributed with $\alpha, \beta, \gamma \sim \mathcal{U}(0, 2\pi)$, $\theta \sim \mathcal{U}(-\Theta/2, \Theta/2)$, and $\phi \sim \mathcal{U}(-\Phi/2, \Phi/2)$, the average polarization matrix for the LoS channel is given by

$$\mathbf{\Lambda} = \begin{bmatrix} \lambda_{11} & \lambda_{12} \\ \lambda_{21} & \lambda_{22} \end{bmatrix}, \quad (24)$$

with its entries defined in (20)-(23), which indicates the average channel gains for the co-polar and cross-polar channels.

Proof: Please refer to the derivations in Section III-B. ■

2) *Depolarization of the NLoS channel:* According to [6], empirical results suggest that the XPD for the scattering NLoS channel maintains a consistent ratio, defined as $\frac{1}{\chi} \triangleq \mathbb{E}\{|d_{\mathcal{V}\mathcal{V}}|^2\}/\mathbb{E}\{|d_{\mathcal{V}\mathcal{H}}|^2\} = \mathbb{E}\{|d_{\mathcal{H}\mathcal{H}}|^2\}/\mathbb{E}\{|d_{\mathcal{H}\mathcal{V}}|^2\}$.

For example, as the XPD approaches infinity, there is no depolarization in the NLoS channel. Moreover, the CPR is assumed to be one, i.e., $\mathbb{E}\{|d_{\nu\nu}|^2\} = \mathbb{E}\{|d_{\mathcal{H}\mathcal{H}}|^2\}$. As a result, the polarization matrix for the NLoS channel is given by

$$\mathbf{\Psi} = \sqrt{\frac{1}{\chi+1}} \begin{bmatrix} 1 & \sqrt{\chi} \\ \sqrt{\chi} & 1 \end{bmatrix}. \quad (25)$$

We note that the normalization above is motivated by power or energy conservation arguments with $\|\mathbf{\Psi}\|_F^2 = \|\mathbf{I}_2\|_F^2 = 2$. In other words, the channel cannot introduce more energy to the transmitted signal and, with this normalization, the power is preserved by deducting the amount of power that leaks into the cross-polar component from the co-polar component.

C. Performance of Polarforming Under Stochastic Channel

In this subsection, we consider the stochastic performance of polarforming in an isotropic scattering environment with an infinite number of NLoS paths. In such an environment, it is reasonable to model the elements of $\tilde{\mathbf{H}}$ as i.i.d. CSCG random variables with normalized covariances as given by (25), i.e., $d_{\nu\nu}, d_{\mathcal{H}\mathcal{H}} \sim \mathcal{CN}(0, \frac{1}{\chi+1})$ and $d_{\mathcal{H}\nu}, d_{\nu\mathcal{H}} \sim \mathcal{CN}(0, \frac{\chi}{\chi+1})$. Without loss of generality, we define the Rician factor, $\kappa \triangleq |\nu|^2/\sigma^2$, to denote the power ratio between the LoS and NLoS components, where σ is the pass loss factor of the NLoS channel. Therefore, the channel matrix can be written in a normalized form as

$$\mathbf{H} = \sqrt{\frac{\kappa}{\kappa+1}} \bar{\mathbf{H}} + \sqrt{\frac{1}{\kappa+1}} \tilde{\mathbf{H}}, \quad (26)$$

where $\bar{\mathbf{H}} = \mathbf{Q}\mathbf{P}e^{j\bar{\psi}}$ with a random phase change $\bar{\psi}$.

The EPSV in (13) can be decomposed into its LoS and NLoS components, i.e., $\mathbf{b} = \mathbf{a} + \mathbf{d}$, where $\mathbf{a} = \sqrt{\frac{\kappa}{\kappa+1}} \bar{\mathbf{H}}\mathbf{f}(\mathbf{t}_0) \triangleq [a_1, a_2]^T$ represents the deterministic LoS component, and $\mathbf{d} = \sqrt{\frac{1}{\kappa+1}} \tilde{\mathbf{H}}\mathbf{f}(\mathbf{t}_0) \triangleq [d_1, d_2]^T$ represents the scattering NLoS component. Since each element of \mathbf{d} is a linear combination of independent CSCG random variables, \mathbf{d} itself is also CSCG distributed. Specifically, $d_\ell \sim \mathcal{CN}(0, \sigma_\ell^2)$, $\ell = 1, 2$, where $\sigma_1^2 = \frac{1}{\kappa+1}(\frac{1}{\chi+1} \cos^2 \rho_{t_0} + \frac{\chi}{\chi+1} \sin^2 \rho_{t_0})$ and $\sigma_2^2 = \frac{1}{\kappa+1}(\frac{\chi}{\chi+1} \cos^2 \rho_{t_0} + \frac{1}{\chi+1} \sin^2 \rho_{t_0})$. With these conditions, the variable $|b_\ell|$ follows a Rician distribution with the probability density function (PDF), i.e.,

$$f_\ell(t) = \frac{2t}{\sigma_\ell^2} e^{-\frac{t^2 + \nu_\ell^2}{\sigma_\ell^2}} I_0\left(\frac{2\nu_\ell t}{\sigma_\ell^2}\right), \quad t \geq 0, \quad \ell = 1, 2, \quad (27)$$

where $\nu_\ell = |a_\ell|$, $\ell = 1, 2$ is the non-centrality parameter. The function $I_0(\cdot)$ is the modified Bessel function of the first kind with order zero.

1) *Relative SNR Gain:* As has been derived in Section III-A, the maximum channel gain of the RPA system through receive polarforming, $|b_1|^2 + |b_2|^2$, can be always achieved by reconfiguring the receive APV to $\rho_r = \tan^{-1}(|b_2|/|b_1|)$ and $\psi_r = \text{mod}\{\omega_1 - \omega_2, 2\pi\}$. The expected value of the maximum channel gain is given by

$$J_{\max} = \mathbb{E}\{|b_1|^2 + |b_2|^2\} = \mathbb{E}\{|b_1|^2\} + \mathbb{E}\{|b_2|^2\} \triangleq \xi_1 + \xi_2, \quad (28)$$

where $\xi_\ell = \nu_\ell^2 + \sigma_\ell^2$, $\ell = 1, 2$ represents the covariance of the Rician-distributed random variable.

For the FPA system, the expected value of the channel gain with the fixed receive APV, $\mathbf{r}_0 = [\rho_{r_0}, \psi_{r_0}]^T$, is written as

$$\begin{aligned} J_{\text{FPA}} &= \mathbb{E}\left\{|\cos \rho_{r_0} b_1 + \sin \rho_{r_0} b_2 e^{j\psi_{r_0}}|^2\right\} \\ &= \cos^2 \rho_{r_0} \mathbb{E}\{|b_1|^2\} + \sin^2 \rho_{r_0} \mathbb{E}\{|b_2|^2\} \\ &\quad + \cos \rho_{r_0} \sin \rho_{r_0} (\mathbb{E}\{b_1 b_2^*\} e^{-j\psi_{r_0}} + \mathbb{E}\{b_1^* b_2\} e^{j\psi_{r_0}}), \end{aligned} \quad (29)$$

where the third term is the correlation of the channels. The cross-term $\mathbb{E}\{b_1 b_2^*\}$ simplifies to $a_1 a_2^*$ due to the independence and zero mean of the random variables b_1 and b_2 . Similarly, $\mathbb{E}\{b_1^* b_2\} = a_1^* a_2$. Thus, by further expanding the correlation term, we obtain

$$\begin{aligned} \Xi &= \cos \rho_{r_0} \sin \rho_{r_0} (a_1 a_2^* e^{-j\psi_{r_0}} + a_1^* a_2 e^{j\psi_{r_0}}) \\ &= \frac{\kappa}{\kappa+1} \cos \rho_{r_0} \sin \rho_{r_0} \\ &\quad \times [a_{\nu\nu} a_{\mathcal{H}\mathcal{H}} \cos^2 \rho_{t_0} \cos \psi_{r_0} \\ &\quad + a_{\mathcal{H}\nu} a_{\mathcal{H}\mathcal{H}} \sin^2 \rho_{t_0} \cos \psi_{r_0} \\ &\quad + a_{\mathcal{H}\nu} a_{\nu\mathcal{H}} \cos \rho_{t_0} \sin \rho_{t_0} \cos(\psi_{t_0} - \psi_{r_0}) \\ &\quad + a_{\mathcal{H}\mathcal{H}} a_{\nu\nu} \cos \rho_{t_0} \sin \rho_{t_0} \cos(\psi_{t_0} - \psi_{r_0})]. \end{aligned} \quad (30)$$

Substituting Ξ into (29), we obtain

$$J_{\text{FPA}} = \xi_1 \cos^2 \rho_{r_0} + \xi_2 \sin^2 \rho_{r_0} + \Xi. \quad (31)$$

The maximized average SNR is given by

$$\max_{\mathbf{r} \in \mathcal{C}_r} \mathbb{E}\{\gamma(\mathbf{t}_0, \mathbf{r})\} = \max_{\mathbf{r} \in \mathcal{C}_r} \mathbb{E}\left\{\frac{|h(\mathbf{t}_0, \mathbf{r})|^2 P_t}{\sigma_n^2}\right\} = \frac{J_{\max} P_t}{\delta^2}, \quad (32)$$

while the average SNR of the FPA system is $\mathbb{E}\{\gamma(\mathbf{t}_0, \mathbf{r}_0)\} = J_{\text{FPA}} P_t / \delta^2$. The relative SNR gain of polarforming compared to the FPA system in the Rician fading channel can be expressed as

$$G_r = \frac{J_{\max}}{J_{\text{FPA}}} = \frac{\xi_1 + \xi_2}{\xi_1 \cos^2 \rho_{r_0} + \xi_2 \sin^2 \rho_{r_0} + \Xi}. \quad (33)$$

As can be seen from (33), the relative gain is closely tied to the type of antenna polarization. To effectively compare and evaluate the benefits of polarforming, we will focus on two commonly used antenna polarization, i.e., linear polarization and circular polarization. In the absence of channel depolarization, optimal transmission in the FPA system is achieved when the transmit and receive antennas share identical polarization. Therefore, we consider the FPA systems, specifically the vertically polarized antenna (VPA) and right-handed circularly polarized antenna (RCPA) systems, both featuring the same polarization for the transmit and receive antennas, i.e., $\mathbf{t}_0 = \mathbf{r}_0$.

For the VPA system, substituting $\mathbf{t}_0 = \mathbf{r}_0 = [0, 0]^T$ into (33), the relative SNR gain achieved by polarforming over the VPA system can be formulated as

$$G_1 = 1 + \frac{(\chi+1) \kappa a_{\mathcal{V}\mathcal{H}}^2 + \chi}{(\chi+1) \kappa a_{\mathcal{V}\mathcal{V}}^2 + 1}. \quad (34)$$

For the RCPA system, after applying $\mathbf{t}_0 = \mathbf{r}_0 = [\pi/4, \pi/2]^T$ into (33), the relative SNR gain achieved by polarforming over the RCPA system is given by

$$G_2 = \frac{2\kappa \sum_{i,j \in \{\mathcal{V}, \mathcal{H}\}} a_{ij}^2 + 2}{\kappa \left(2a_{\mathcal{V}\mathcal{V}}a_{\mathcal{H}\mathcal{H}} - 2a_{\mathcal{V}\mathcal{H}}a_{\mathcal{H}\mathcal{V}} + \sum_{i,j \in \{\mathcal{V}, \mathcal{H}\}} a_{ij}^2 \right) + 1}. \quad (35)$$

When the Euler angles and AoAs are fixed, the corresponding coefficients a_{ij} , $i, j \in \{\mathcal{V}, \mathcal{H}\}$ remain constant. The depolarization of the LoS channel can change the relative SNR gain to the extent of this effect dictated by the Rician κ -factor. In the VPA system, the XPD of the NLoS channel plays a significant role, whereas the RCPA system is not affected by this factor. When $\kappa = 0$, the channel behaves as a Rayleigh fading channel, where $G_1 = 1 + \frac{1}{\chi}$ and $G_2 = 2$. It indicates that, compared to the VPA system, the relative SNR gain is related to the depolarization of the NLoS channel. However, compared to the RCPA system, the gain is fixed at two, which demonstrates that polarforming can always combat the depolarization effects in the NLoS channel.

2) *CDF Performance*: Furthermore, the CDF of the maximum channel gain for the Rician fading channel can be expressed as

$$F(t) = \Pr \left\{ |b_1|^2 + |b_2|^2 \leq t \right\} \\ = \int_0^q \int_0^p f_1(x)f_2(y) dx dy, \quad t \geq 0, \quad (36)$$

where $p = \sqrt{t - y^2}$ and $q = \sqrt{t}$. The integration in (36) is challenging to derive in an exact closed-form owing to the difficulty of expressing the distribution of $|b_1|^2 + |b_2|^2$ as a simple function. However, we can approximate it using Gauss-Chebyshev quadrature method [34] as follows.

By leveraging change of variables, where $u = 2x/p - 1$ and $v = 2y/q - 1$, we have $dx = \frac{p}{2} du$ and $dy = \frac{q}{2} dv$. Substituting these into (36), we obtain

$$F(t) = \int_{-1}^{+1} \int_{-1}^{+1} \frac{pq}{4} f_1 \left(\frac{pu + p}{2} \right) f_2 \left(\frac{qv + q}{2} \right) dudv, \\ t \geq 0. \quad (37)$$

Applying the Gauss-Chebyshev quadrature method, the CDF of the maximum channel gain can be approximated as

$$F(t) \approx \frac{\pi^2 t}{8N^2} \sum_{i,j=1}^N \sqrt{(1 - u_i^2)(1 - v_j^2)(3 - v_j^2 - 2v_j)} \\ \times f_1 \left(\frac{(1 + u_i) \sqrt{3 - v_j^2 - 2v_j}}{4} \sqrt{t} \right) f_2 \left(\frac{(1 + v_j) \sqrt{t}}{2} \right), \\ t \geq 0, \quad (38)$$

where $u_i = \cos((i - 1/2)\pi/N)$, $v_j = \cos((j - 1/2)\pi/N)$, and N is the number of samples used to balance the tradeoff between computational complexity and accuracy.

The outage probability is defined as the probability that the SNR γ falls below a required threshold t , i.e.,

$$P_{\text{out}}(t) = \Pr \{ \gamma \leq t \} = F \left(\frac{\delta^2 t}{P_t} \right), \quad t \geq 0. \quad (39)$$

As an example, for any given transmit power P_t , noise power δ^2 , and receive SNR threshold γ_{th} , the outage probability for the RPA system under the Rician fading channel is given by $F(\delta^2 \gamma_{\text{th}}/P_t)$.

3) *Polarforming Diversity*: To analyze the diversity gain of polarforming, we assume the system operates in a high SNR regime (corresponding to small t). In this regime, the Bessel function $I_0(x)$ can be approximated by $I_0(x) \approx 1$ for small x . Therefore, at high SNR, the PDF of the Rician fading channel in (27) can be approximated by

$$f_\ell(t) \approx \frac{2t}{\sigma_\ell^2} e^{-\frac{v_\ell^2}{\sigma_\ell^2}}, \quad t \geq 0, \quad \ell = 1, 2. \quad (40)$$

Substituting this approximation into (38), the error probability for the RPA system at high SNR ρ is then calculated as

$$P_e(\rho) \approx \int_0^{\frac{1}{\rho}} dF(t) \\ = \frac{\pi^2 \delta^4}{8P_t^2 N^2 \rho} \sum_{i,j=1}^N \sqrt{(1 - u_i^2)(1 - v_j^2)(3 - v_j^2 - 2v_j)} \\ \times \frac{(1 + u_i) \sqrt{(3 - v_j^2 - 2v_j)}}{2\sigma_1^2 \sqrt{\rho}} e^{-\frac{v_i^2}{\sigma_1^2}} \times \frac{(1 + v_j)}{\sigma_2^2 \sqrt{\rho}} e^{-\frac{v_j^2}{\sigma_2^2}} \\ = \frac{\pi^2 \delta^4}{16\sigma_1^2 \sigma_2^2 P_t^2 N^2 \rho^2} e^{-\frac{v_1^2}{\sigma_1^2} - \frac{v_2^2}{\sigma_2^2}} \sum_{i,j=1}^N \sqrt{(1 - u_i^2)(1 - v_j^2)} \\ \times (1 + u_i)(1 + v_j)(3 - v_j^2 - 2v_j) \\ \triangleq \frac{C}{\rho^2}, \quad (41)$$

where C is a constant.

The diversity gain/order G_d is defined as the negative slope of the error probability versus the SNR on a logarithmic scale in the regime of asymptotically large ρ . Specifically,

$$G_d = - \lim_{\rho \rightarrow \infty} \frac{\log_2 P_e(\rho)}{\log_2 \rho} = \lim_{\rho \rightarrow \infty} \frac{2 \log_2 \rho - \log_2 C}{\log_2 \rho} = 2. \quad (42)$$

Thus, the diversity gain/order of polarforming using dual-polarized antennas is two, indicating that the proposed system can effectively combat the impact of fading on the error rate by leveraging two independent diversity branches.

D. Practical Considerations

In this subsection, we discuss the practical aspects of polarforming that may influence its effectiveness.

1) *Antenna Cross-Polar Isolation (XPI)*: Ideally, a polarized antenna generates an oscillating electric field only along its designated orientation without any components leaking into the orthogonal orientation. However, in practical antenna design, cross-polar leakages inevitably occur due to imperfections in the antenna architecture and design. Such leakages are well-known in antenna theory [35] and are often characterized using antenna XPI. Analytically, the presence of leakages can contribute to depolarization effects in both LoS and NLoS

channels. To account for this impact, the channel matrix can be modeled as [36]

$$\mathbf{H}_a = \mathbf{X}_r \mathbf{H} \mathbf{X}_t, \quad (43)$$

where the coupling matrices of the transmit and receive antennas with normalized channel power are expressed as

$$\mathbf{X}_t = \sqrt{\frac{1}{\mu_t + 1}} \begin{bmatrix} 1 & \sqrt{\mu_t} \\ \sqrt{\mu_t} & 1 \end{bmatrix}, \quad (44)$$

$$\mathbf{X}_r = \sqrt{\frac{1}{\mu_r + 1}} \begin{bmatrix} 1 & \sqrt{\mu_r} \\ \sqrt{\mu_r} & 1 \end{bmatrix}. \quad (45)$$

Here, $1/\mu_t$ and $1/\mu_r$ represent the antenna XPI capability of the transmit and receive dual-polarized antennas, respectively, where μ_t and μ_r do not exceed one.

2) *Channel Correlation*: In wireless communication systems, when the scattering is insufficient to decorrelate the channels, the elements of \mathbf{H} will be correlated. This correlation may deteriorate the performance of a polarized antenna system by reducing its ability to effectively separate signals. To account for this, we consider the correlation at the transmitter and receiver and thus, the channel matrix for the NLoS component is given by [37]

$$\tilde{\mathbf{H}}_c = \mathbf{C}_r^{1/2} \tilde{\mathbf{H}} \mathbf{C}_t^{1/2}, \quad (46)$$

where $\tilde{\mathbf{H}}$ is the uncorrelated channel matrix in (26), and \mathbf{C}_r and \mathbf{C}_t are the receive and transmit correlation matrices, respectively. The transmit and receive correlation matrices are defined as

$$\mathbf{C}_t = \begin{bmatrix} 1 & t_p \\ t_p^* & 1 \end{bmatrix} \text{ and } \mathbf{C}_r = \begin{bmatrix} 1 & r_p \\ r_p^* & 1 \end{bmatrix}, \quad (47)$$

where $t_p \triangleq \frac{\chi+1}{\sqrt{\chi}} \mathbb{E} \{d_{\mathcal{V}\mathcal{V}} d_{\mathcal{H}\mathcal{V}}^*\} = \frac{\chi+1}{\sqrt{\chi}} \mathbb{E} \{d_{\mathcal{V}\mathcal{H}} d_{\mathcal{H}\mathcal{H}}^*\}$ and $r_p \triangleq \frac{\chi+1}{\sqrt{\chi}} \mathbb{E} \{d_{\mathcal{V}\mathcal{V}} d_{\mathcal{V}\mathcal{H}}^*\} = \frac{\chi+1}{\sqrt{\chi}} \mathbb{E} \{d_{\mathcal{H}\mathcal{V}} d_{\mathcal{H}\mathcal{H}}^*\}$ represent the complex-valued correlation coefficients at the transmitter and receiver, respectively.

3) *Implementation Issue of Polarformers*: A straightforward method for altering the antenna polarization in the RPA system is to use a polarformer including phase shifters and attenuators, as depicted in Fig. 1. The phase shifters and attenuators enable precise polarization control by adjusting the phase and amplitude of the signals. However, this method comes with the cost of requiring a dedicated control circuit to manage the phase shifters and attenuators, which can add to the hardware and implementation complexity. Other viable alternatives, such as MEMS-based antennas, reconfigurable antennas, or metasurfaces, provide different avenues for polarization control and have been discussed in Section I. The selection of a polarization tuning method generally involves a tradeoff between cost, implementation complexity, and precision, which makes it essential to consider the specific requirements of the application.

4) *Polarization Channel Estimation*: Channel state information (CSI) is essential for optimizing the system performance, as its accuracy directly influences the effectiveness of polarforming. Precise CSI allows the system to better adapt to channel depolarization and variations, thereby fully exploiting polarization diversity. Common channel estimation

techniques, such as least squares (LS), minimum mean square error (MMSE), and maximum likelihood (ML) estimation, present different tradeoffs between computational complexity and estimation accuracy [38]. For the considered RPA system, a key challenge is to estimate the CSI of a two-by-two channel matrix, which differs from conventional systems. Specifically, it requires separate estimation of the CSIs for co-polar and cross-polar channels and hence leads to a fourfold increase in the number of pilots needed. It will be interesting to devise new methods to acquire the CSI of polarization channels more efficiently in future work.

IV. SIMULATION RESULTS

Extensive simulations are carried out in this section to evaluate the performance gains of the proposed system over conventional FPA systems and to verify our analytical results.

In the simulation, the polarization of the transmit antenna is kept fixed, following the simplification discussed in Section III, while the receive antenna flexibly operates within the tunable APV region $\mathcal{C}_p = [0, \pi/2] \times [0, 2\pi]$. This setup allows us to analyze the effects of varying the antenna polarization at the receiver, where receive polarforming is employed. The Euler angles α, β, γ and physical AoAs of the LoS path θ, ϕ are modeled as i.i.d. and uniformly distributed random variables with $\alpha, \beta, \gamma \sim \mathcal{U}(0, 2\pi)$, $\theta \sim \mathcal{U}(-\Theta/2, \Theta/2)$, and $\phi \sim \mathcal{U}(-\Phi/2, \Phi/2)$. The coverage angles are set to $\Theta = \Phi = \pi$, which corresponds to a scenario with broad angular coverage and allows the incoming EM wave of the LoS path to arrive from a wide range of directions. This section evaluates the average performance of the system considering the random Euler angles and AoAs. Further, the channel coefficients of the NLoS channel are assumed to be i.i.d. CSCG-distributed random variables. Specifically, the co-polar components $d_{\mathcal{V}\mathcal{V}}$ and $d_{\mathcal{H}\mathcal{H}}$ follow the distribution $\mathcal{CN}(0, \frac{1}{\chi+1})$, while the cross-polar components $d_{\mathcal{H}\mathcal{V}}$ and $d_{\mathcal{V}\mathcal{H}}$ follow the distribution $\mathcal{CN}(0, \frac{\chi}{\chi+1})$. For convenience, we assume the ratio of the average received signal power to noise power is normalized to $\frac{P_s \sigma_p^2}{\delta^2} = 1$. To ensure the robustness of simulations, the results are carried out based on 10^5 Monte Carlo simulations with independent realizations.

In comparison to the proposed RPA system, three benchmark schemes are defined below.

- **Linearly polarized antenna (LPA)**: The transmit and receive antennas are both fixed with linear polarization, i.e., vertical polarization as discussed in Section III-B. In other words, the transmit and receive APVs are set to $\mathbf{t}_0 = \mathbf{r}_0 = [0, 0]^T$.
- **Circularly polarized antenna (CPA)**: The polarization of both the transmitter and receiver is configured for circular polarization, i.e., right-handed circular polarization as discussed in Section III-B. In this setup, the transmit and receive APVs are given by $\mathbf{t}_0 = \mathbf{r}_0 = [\pi/4, \pi/2]^T$.
- **Digital Beamforming (DBF)**: This scheme considers a single-input multiple-output (SIMO) system where the receiver uses M RF chains and an antenna array with M antennas. Each antenna has the same polarization as the transmitter and is spaced half a wavelength apart. In

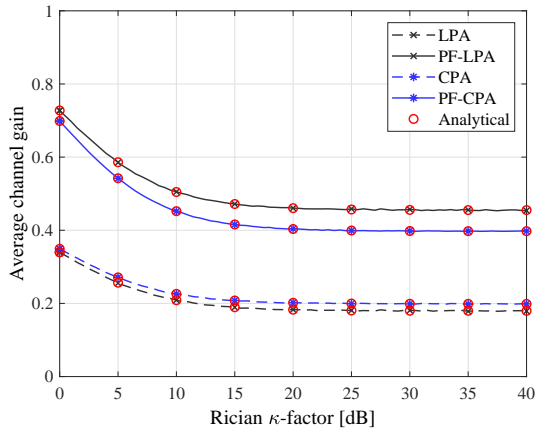


Fig. 6. Comparison of average channel gains for LPA, CPA, and the proposed schemes with the XPD $1/\chi = 0$ dB.

this configuration, maximum ratio combining (MRC) is applied at the receiver to achieve the maximum SNR.

For each of the above benchmark schemes, we introduce the corresponding RPA-aided scheme, referred to as PF-LPA, PF-CPA, and PF-DBF, respectively. These schemes allow the receive RPAs to dynamically adjust their polarization to optimize performance.

Fig. 6 shows the average channel gains for LPA, CPA, and the proposed schemes with the XPD set to $1/\chi = 0$ dB. The solid and dashed lines represent Monte Carlo simulation results based on random Euler angles and AoAs, and the analytical results are derived from Theorem 1. As can be seen in the figure, the proposed schemes, PF-LPA and PF-CPA, consistently outperform their FPA counterparts, LPA and CPA, across all values of the Rician κ -factor. The performance improvement is due to the ability of polarforming to dynamically adjust the polarization to maximize the channel gain, effectively leveraging the additional DoFs provided by polarization diversity. Interestingly, the average channel gain decreases as the Rician κ -factor increases. This is because the depolarization effect in the LoS channel is stronger than in the NLoS channel when $1/\chi = 0$ dB. In other words, at higher Rician κ -factors, the dominant LoS component experiences more significant depolarization compared to the NLoS components, which leads to a reduction in channel power and consequently degrades performance. The figure also confirms that the analytical results derived from Theorem 1 are in precise match with the simulation results for average channel gain. This exact match validates the accuracy of the theoretical derivations presented in earlier sections. Given this validation, Theorem 1 can be used to predict the average performance of the proposed system, which can provide a considerable reduction in simulation time without sacrificing accuracy. This efficiency is especially beneficial in scenarios where extensive simulations are computationally demanding. For this reason, Theorem 1 is employed in the subsequent simulations.

Fig. 7 compares the relative SNR gains for DBF and the proposed schemes across various Rician κ -factors of $\kappa = 0$,

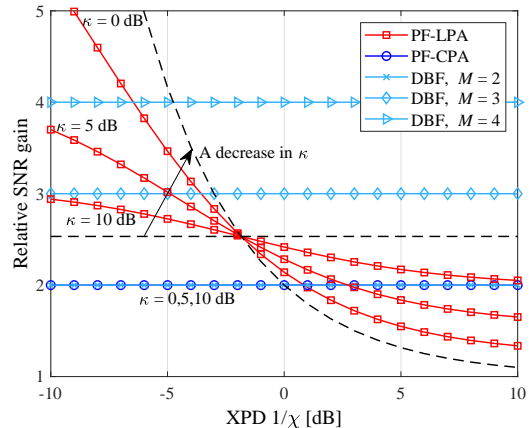


Fig. 7. Comparison of relative SNR gains for DBF and the proposed schemes.

5, and 10 dB. It can be observed that under conditions of poor XPD (indicating severe depolarization), the PF-LPA scheme can achieve a higher relative SNR gain than the DBF scheme with multiple antennas. This advantage arises because PF-LPA benefits from greater polarization diversity, which allows it to effectively combat depolarization effects in the channel. While DBF can exploit spatial DoFs to enhance system performance, its effectiveness is limited in environments with severe depolarization for the schemes deploying LPA. An interesting observation is the presence of a crossover point for the PF-LPA scheme with different Rician κ -factors. This point corresponds to the relative SNR gain in the LoS channel, which implies a shift in depolarization dominance as the XPD varies. This behavior suggests that the advantage of polarforming for the PF-LPA scheme depends on both the Rician κ -factor and the XPD level. On the other hand, the PF-CPA scheme exhibits the relative SNR gain of two, regardless of the Rician κ -factor or the XPD. It implies that the performance of polarforming for the scheme using CPA is robust to changes in channel conditions caused by altering Rician κ -factors and depolarization levels. Remarkably, the PF-CPA scheme achieves the same relative SNR gain as DBF with $M = 2$ antennas. This finding reveals that the RPA system can potentially save antenna spacing in MIMO systems and provide a compact yet efficient alternative to traditional DBF systems.

Fig. 8 illustrates the comparative performance of CDFs for CPA, DBF, and the proposed schemes under various channel conditions, including Rician fading channels with $\kappa = 5$ dB and $\kappa = 0$ dB, as well as the Rayleigh fading channel, with the XPD $1/\chi = 0$ dB. In this figure, the simulated CDF of the proposed system has a perfect match compared to the approximated one ($N = 20$). It indicates that (38) provides a good approximation for the CDF of the maximum channel gain and can be utilized for analyzing the outage probability for the RPA system. The proposed schemes, PF-CPA and PF-DBF, outperform the CPA and DBF schemes across all considered channel conditions, as evidenced by their CDF curve lying to the left of the others. It indicates that the RPA system can always achieve a lower outage

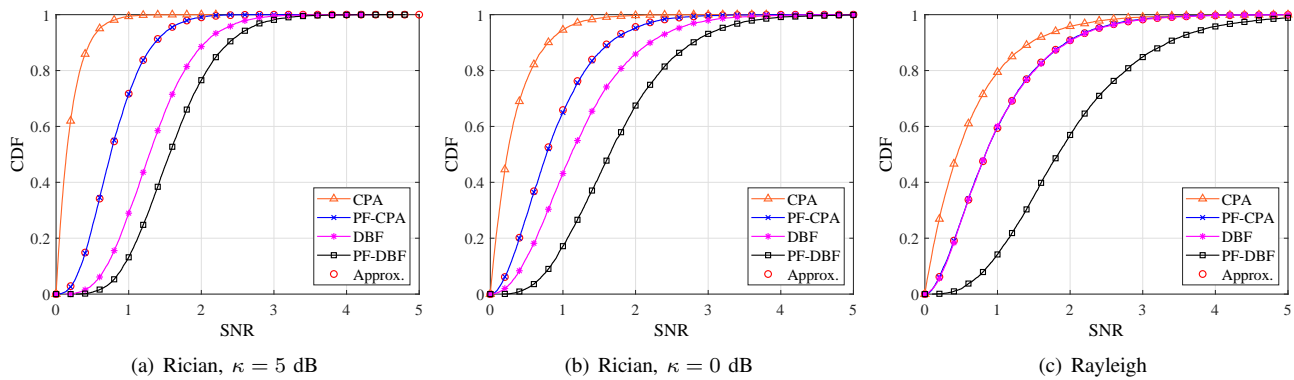


Fig. 8. Comparisons of CDFs for CPA, DBF, and the proposed schemes with the XPD $1/\chi = 0$ dB.

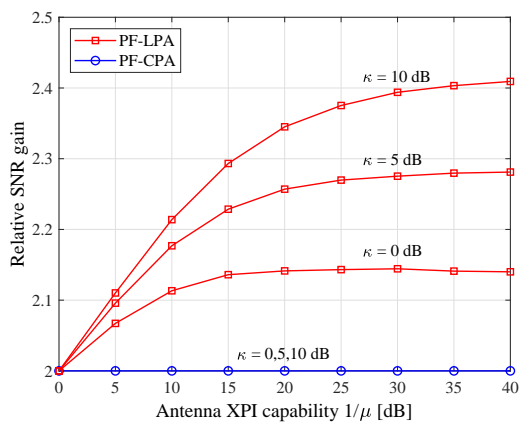


Fig. 9. Impact of antenna XPI on the proposed schemes with the XPD $1/\chi = 0$ dB.

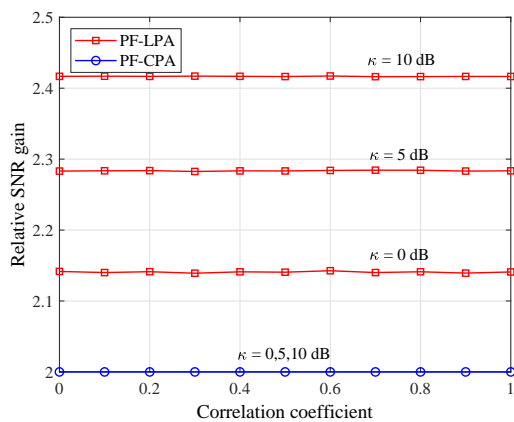


Fig. 10. Impact of channel correlation on the proposed schemes with the XPD $1/\chi = 0$ dB under the assumption of $t_p = r_p$.

probability for any SNR threshold. Notably, in the Rician fading channel, the performance advantage of PF-CPA over the other schemes becomes more significant as the Rician factor decreases. In Figs. 8(a) and 8(b), the performance gap widens at $\kappa = 0$ dB compared to $\kappa = 5$ dB because the dominant depolarization effect in the LoS component degrades overall system performance when $1/\chi = 0$ dB. For the Rayleigh fading channel, as shown in Fig. 8(c), while the differences between the schemes are less pronounced, PF-CPA and PF-DBF still show superior performance compared to the CPA and DBF schemes. In particular, the PF-CPA scheme matches the performance of DBF, which confirms that both the polarization diversity of two and the spatial diversity of two are fully exploited.

Figs. 9 and 10 depict the impacts of antenna XPI and channel correlation on the proposed schemes with the XPD $1/\chi = 0$ dB for different Rician κ -factors $\kappa = 0, 5, \text{ and } 10$ dB. In Fig. 9, the relative SNR gain of the PF-LPA scheme increases as the antenna XPI capability improves, particularly for higher Rician κ -factors. The trend indicates that PF-LPA is sensitive to XPI capability, especially in environments with a strong LoS component. Enhancing XPI capability by reducing antenna cross-polar leakage can therefore significantly improve the performance of the proposed system. In contrast, the

PF-CPA scheme exhibits a flat response across all XPI levels, which demonstrates its robustness and consistent performance regardless of the antenna XPI capability. This suggests that PF-CPA can maintain optimal performance even with limited XPI capability. Fig. 10 further shows that both PF-LPA and PF-CPA maintain steady relative SNR gains across different levels of channel correlation. This stability suggests that channel correlation has little impact on the performance of the proposed schemes, thereby reinforcing their reliability under varying correlation conditions. The consistent performance of the PF-CPA scheme across both figures highlights its suitability for environments where XPI and correlation levels are variable, as it can always achieve the maximum achievable SNR gains. On the other hand, PF-LPA provides greater advantages in scenarios where XPI can be effectively controlled or optimized, especially in situations with strong LoS components that benefit from enhanced polarization management. Overall, these findings suggest that PF-CPA is a robust choice for systems with limited XPI capability and varying channel correlation conditions, and it can deliver reliable performance across diverse scenarios. In contrast, PF-LPA offers superior performance gains when XPI and XPD are well-managed, and this makes it ideal for specific deployments in suitable wireless environments.

V. CONCLUSION

In this paper, we introduced and studied the concept of polarforming that allows flexible adjustment of antenna polarization to improve the performance of wireless communications systems. To accurately capture the effects of depolarization, especially in the LoS channel, we developed a comprehensive wavefront-based channel model. Based on this model, we provided detailed descriptions of both transmit and receive polarforming and analytically characterized the depolarization effects in both LoS and NLoS channels. Furthermore, we derived the relative SNR gain in closed-form under the stochastic channel and approximated the CDF of the maximum channel gain achieved by polarforming. The analytical results revealed that the proposed system can fully exploit polarization diversity due to a polarforming diversity gain of two. Extensive simulation results demonstrated the effectiveness of polarforming compared to the FPA systems and verified our analytical analysis. The results also showed that the RPA-aided systems can not only better combat channel depolarization, but also adapt to channel variations more efficiently.

REFERENCES

- [1] M. R. Andrews, P. P. Mitra, and R. deCarvalho, "Tripling the capacity of wireless communications using electromagnetic polarization," *Nature*, vol. 409, pp. 316–318, Jan. 2001.
- [2] M. Aldababsa, S. Özyurt, G. K. Kurt, and O. Kucur, "A survey on orthogonal time frequency space modulation," *IEEE Open J. Commun. Soc.*, vol. 5, pp. 4483–4518, 2024.
- [3] T. S. Rappaport, Y. Xing, O. Kanhere, S. Ju, A. Madanayake, S. Mandal, A. Alkhateeb, and G. C. Trichopoulos, "Wireless communications and applications above 100 GHz: Opportunities and challenges for 6G and beyond," *IEEE Access*, vol. 7, pp. 78729–78757, 2019.
- [4] E. G. Larsson, O. Edfors, F. Tufvesson, and T. L. Marzetta, "Massive MIMO for next generation wireless systems," *IEEE Commun. Mag.*, vol. 52, no. 2, pp. 186–195, Feb. 2014.
- [5] F. Mani and C. Oestges, "A ray based indoor propagation model including depolarizing penetration," in *Proc. 3rd Eur. Conf. Antennas and Propagation*, Mar. 2009, pp. 3835–3838.
- [6] Y. He, X. Cheng, and G. L. Stüber, "On polarization channel modeling," *IEEE Wireless Commun.*, vol. 23, no. 1, pp. 80–86, Feb. 2016.
- [7] R. U. Nabar, H. Bolcskei, V. Erceg, D. Gesbert, and A. J. Paulraj, "Performance of multiantenna signaling techniques in the presence of polarization diversity," *IEEE Trans. Signal Process.*, vol. 50, no. 10, pp. 2553–2562, Oct. 2002.
- [8] H. Asplund, J.-E. Berg, F. Harrysson, J. Medbo, and M. Riback, "Propagation characteristics of polarized radio waves in cellular communications," in *Proc. IEEE VTC*, Baltimore, MD, USA, 2007, pp. 839–843.
- [9] V. Nikolaidis, N. Moraitis, and A. G. Kanatas, "Dual-polarized narrow-band MIMO LMS channel measurements in urban environments," *IEEE Trans. Antennas Propag.*, vol. 65, no. 2, pp. 763–774, Feb. 2017.
- [10] Y. Yao, F. Shu, Z. Li, X. Cheng, and L. Wu, "Secure transmission scheme based on joint radar and communication in mobile vehicular networks," *IEEE Trans. Intell. Transp. Syst.*, vol. 24, no. 9, pp. 10027–10037, Sep. 2023.
- [11] K. Meng, Q. Wu, J. Xu, W. Chen, Z. Feng, R. Schober, and A. L. Swindlehurst, "UAV-enabled integrated sensing and communication: Opportunities and challenges," *IEEE Wireless Commun.*, vol. 31, no. 2, pp. 97–104, Jul. 2024.
- [12] Y. P. Selvam, L. Elumalai, M. G. N. Alsath, M. Kanagasabai, S. Subbaraj, and S. Kingsly, "Novel frequency- and pattern-reconfigurable rhombic patch antenna with switchable polarization," *IEEE Antennas Wireless Propag. Lett.*, vol. 16, pp. 1639–1642, 2017.
- [13] Y. Al-Yasir, A. Abdullah, N. O. Parchin, R. Abd-Alhameed, and J. Noras, "A new polarization-reconfigurable antenna for 5G applications," *Electronics*, vol. 7, no. 11, p. 293, Nov. 2018.
- [14] P. K. Li, Z. H. Shao, Q. Wang, and Y. J. Cheng, "Frequency- and pattern-reconfigurable antenna for multistandard wireless applications," *IEEE Antennas Wireless Propag. Lett.*, vol. 14, pp. 333–336, 2015.
- [15] S.-A. Malakooti and C. Fumeaux, "Pattern-reconfigurable antenna with switchable wideband to frequency-agile bandpass/bandstop filtering operation," *IEEE Access*, vol. 7, pp. 167065–167075, 2019.
- [16] I. T. Nassar, H. Tsang, D. Bardroff, C. P. Lusk, and T. M. Weller, "Mechanically reconfigurable, dual-band slot dipole antennas," *IEEE Trans. Antennas Propag.*, vol. 63, no. 7, pp. 3267–3271, Jul. 2015.
- [17] J. Costantine, Y. Tawk, J. Woodland, N. Flaum, and C. G. Christodoulou, "Reconfigurable antenna system with a movable ground plane for cognitive radio," *IET Microw., Antennas Propag.*, vol. 8, no. 11, pp. 858–863, Aug. 2014.
- [18] T. Li and Z. N. Chen, "A dual-band metasurface antenna using characteristic mode analysis," *IEEE Trans. Antennas Propag.*, vol. 66, no. 10, pp. 5620–5624, Oct. 2018.
- [19] S. S. Syed Nasser, W. Liu, and Z. N. Chen, "Wide bandwidth and enhanced gain of a low-profile dipole antenna achieved by integrated suspended metasurface" *IEEE Trans. Antennas Propag.*, vol. 66, no. 3, pp. 1540–1544, Mar. 2018.
- [20] S. X. Ta and I. Park, "Compact wideband circularly polarized patch antenna array using metasurface," *IEEE Antennas Wireless Propag. Lett.*, vol. 16, pp. 1932–1936, 2017.
- [21] T. Li and Z. N. Chen, "Wideband substrate-integrated waveguide-fed endfire metasurface antenna array," *IEEE Trans. Antennas Propag.*, vol. 66, no. 12, pp. 7032–7040, Dec. 2018.
- [22] N.-S. Nie, X.-S. Yang, Z. N. Chen, and B.-Z. Wang, "A low-profile wideband hybrid metasurface antenna array for 5G and WiFi systems," *IEEE Trans. Antennas Propag.*, vol. 68, no. 2, pp. 665–671, Feb. 2020.
- [23] J. T. S. Do, J. Zang, A. Alvarez-Melcon, and J. S. Gomez-Diaz, "Time-modulated patch antennas with tunable and nonreciprocal polarization response," *IEEE Access*, vol. 10, pp. 59057–59067, 2022.
- [24] L. Zhu, W. Ma, and R. Zhang, "Movable antennas for wireless communication: Opportunities and challenges," *IEEE Commun. Mag.*, vol. 62, no. 6, pp. 114–120, Jun. 2024.
- [25] X. Shao and R. Zhang, "6DMA enhanced wireless network with flexible antenna position and rotation: Opportunities and challenges," arXiv preprint *arXiv:2406.06064*, 2024.
- [26] J. D. Boerman and J. T. Bernhard, "Performance study of pattern reconfigurable antennas in MIMO communication systems," *IEEE Trans. Antennas Propag.*, vol. 56, no. 1, pp. 231–236, Jan. 2008.
- [27] T. Zhao, M. Li, and Y. Pan, "Online learning-based reconfigurable antenna mode selection exploiting channel correlation," *IEEE Trans. Wireless Commun.*, vol. 20, no. 10, pp. 6820–6834, Oct. 2021.
- [28] M. Hasan, I. Bahçeci, and B. A. Cetiner, "Downlink multi-user MIMO transmission for radiation pattern reconfigurable antenna systems," *IEEE Trans. Wireless Commun.*, vol. 17, no. 10, pp. 6448–6463, Oct. 2018.
- [29] Y. Hou, M. Li, and K. Zeng, "Throughput optimization in multi-hop wireless networks with reconfigurable antennas," in *Proc. Int. Conf. Comput., Netw. Commun. (ICNC)*, Jan. 2017, pp. 620–626.
- [30] M. R. Castellanos and R. W. Heath, "Linear polarization optimization for wideband MIMO systems with reconfigurable arrays," *IEEE Trans. Wireless Commun.*, vol. 23, no. 3, pp. 2282–2295, Mar. 2024.
- [31] C. Oestges and B. Clerckx, *MIMO wireless communications: from realworld propagation to space-time code design*. Singapore: Elsevier Sci., 2010.
- [32] J. Diebel, "Representing attitude: Euler angles, unit quaternions, and rotation vectors," *Matrix*, vol. 58, no. 15-16, pp. 1–35, 2006.
- [33] M. -T. Dao, V. -A. Nguyen, Y. -T. Im, S. -O. Park, and G. Yoon, "3D polarized channel modeling and performance comparison of MIMO antenna configurations with different polarizations," *IEEE Trans. Antennas Propag.*, vol. 59, no. 7, pp. 2672–2682, Jul. 2011.
- [34] L. Wei, K. Wang, C. Pan, and M. Elkhshlan, "Average error probability for UAV-RIS enabled short packet communications," *IEEE Trans. Veh. Technol.*, vol. 73, no. 2, pp. 2912–2917, Feb. 2024.
- [35] C. A. Balanis, *Antenna Theory: Analysis and Design*, 4th ed. Hoboken, NJ, USA: Wiley, 2016.
- [36] C. Oestges, B. Clerckx, M. Guillaud, and M. Debbah, "Dual-polarized wireless communications: From propagation models to system performance evaluation," *IEEE Trans. Wireless Commun.*, vol. 7, no. 10, pp. 4019–4031, Oct. 2008.
- [37] M. Coldrey, "Modeling and capacity of polarized MIMO channels," in *Proc. VTC Spring*, May 2008, pp. 440–444.
- [38] D. Tse and P. Viswanath, *Fundamentals of Wireless Communication*. Cambridge, U.K.: Cambridge Univ. Press, 2005.